IN-FLIGHT CALIBRATION OF SPOT5 AND FORMOSAT2

Th. Toutin [a, *], E. Blondel[b], K. Rother[c], S. Mietke[c]

[a] Natural Resources Canada, Canada Centre for Remote Sensing, 588 Booth St., Ottawa, Ontario, K1A 0Y7 Canada - thierry.toutin@ccrs.nrcan.gc.ca

[b] TGIS Technologies Inc., 16 rue Pelletier, Chelsea, Quebec, J9B 2A6 Canada – carbo@tgis.ca

[c] Technische Universität Dresden, Institut für Kartographie, Helmholtzstraße 10, D-01062, Dresden, Germany - Regen_Schauer@gmx.de

Commission I, WG I/5

KEY WORDS: Remote sensing, Geometry, Mapping, Calibration, Correction, SPOT5, Formosat2, Accuracy

ABSTRACT:

The main objectives of this research study were to address the internal orientation of high-resolution sensors, and to perform an in-flight calibration of the SPOT5 HRS/HRG and Formosat2 RSI lenses. The other objectives were to evaluate the impacts of this in-flight calibration on the sensor orientations and elevation extraction. Stereo-extracted elevations were compared to accurate Lidar elevation data. Since the 3D multi-sensor geometric modelling used in the auto-calibration already corrects some of the lens distortions, only the remaining radial and decentering distortions were addressed.

The first results on the lens distortion computation and evaluation have shown that (i) the radial symmetric and asymmetric distortions for SPOT5 HRS and (ii) only the radial symmetric distortions for Formosat2 RSI have to be corrected in order to achieve sub-pixel planimetric accuracy in the sensors orientation. The second results on the stereo-extraction of elevations demonstrated few improvements on their accuracy (less than 0.5 m) for SPOT5 HRS due to the centred and aligned location of CCDs in the *x*-axis focal plane, while the elevation parallax with in-track stereoscopy is in the *y*-axis. On the other hand, the *y*-axis component of radial distortions with Formosat2 RSI due to its ex-centred location in the focal plane generated elevation errors (5 m and more), which were then corrected by the auto-calibration process.

Finally, if sub-pixel accuracy (planimetry and elevation) is not requested for specific applications, the lens calibration could be neglected without degrading the final results at the pixel level. However, the auto-calibration process should be always performed for DEM and ortho-image generation in mountainous areas because the radial distortions affect the sensor orientation (few pixels), which thus generate large errors in elevation. Worse relative results were obtained with Formosat2 than with SPOT5 because there were some inconsistencies in attitude data of our Formosat2 RSI data. These attitude problems should have been now resolved.

RÉSUMÉ :

Les objectifs principaux de cette recherche étaient d'évaluer l'orientation interne de capteurs de haute résolution, et de réaliser un auto-calibrage des lentilles de SPOT5 HRS/HRG et de Formosat2 RSI. Les autres objectifs étaient d'évaluer l'impact de cet auto-calibrage sur l'orientation des capteurs et l'extraction d'altitudes. Les altitudes extraites par stéréoscopie ont été comparées à des données d'altitude Lidar précises. Comme la modélisation géométrique 3D multi-capteur utilisée dans l'auto-calibrage corrige déjà certaines des distorsions de la lentille, seulement les distorsions radiales symétriques, asymétriques et tangentielles ont été évaluées.

Les premiers résultats sur les calculs et l'évaluation des distorsions des lentilles ont démontrés que, pour obtenir une précison planimétrique du sous-pixel dans l'orientation des capteurs, (i) les distorsions radiales symétriques et asymétriques pour SPOT5 HRS et (ii) seulement les distorsions radiales symétriques pour Formosat2 RSI doivent être corrigées. Les seconds résultats sur l'extraction stéréo d'altitude ont démontrés pour SPOT5 HRS peu d'amélioration sur la précision (moins que 0,5 m) car, le capteur est centré et aligné dans l'axe des abscisses du plan focal alors que la parallaxe d'altitude pour une stéréoscopie le long de la trace est dans l'axe des ordonnées. Par contre, la composante en ordonnée de la distorsion radiale pour Formosat2 RSI, à cause de l'excentrement du capteur dans le plan focal, génère des erreurs d'altitude (5 m et plus), qui sont alors corrigées avec l'auto-calibrage.

Quand une application spécifique ne demande pas une précision du sous-pixel (planimétrie et altitude), le calibrage de la lentille peut être ignoré sans affecter les résultats finaux. Par contre, l'auto-calibrage devrait toujours être réalisé pour la création de MNT dans les terrains montagneux, parce que la distorsion radiale affecte l'orientation du capteur de quelques pixels; ce qui crée alors

* Corresponding author: thierry.toutin@ccrs.nrcan.gc.ca.

des erreurs en altitude. De plus mauvais résultats ont été obtenus avec Formosat2 qu'avec SPOT5 à cause de certaines erreurs dans les données d'attitude de nos images Formosat2 RSI. Ces problèmes d'attitude devraient être maintenant réglés.

1. INTRODUCTION

Lenses and imaging systems generally fall into a few major categories in terms of the geometry of the images they produce - rectilinear, fisheye, scanning cameras and various kinds of curved mirror systems. A real-world lens or camera system, except for a pinhole camera, will vary more or less in its actual image geometry from its ideal type. Lens distortion causes thus imaged positions to be displaced from their ideal locations, and the geometry quality of the image is also deteriorated. The process of measurement of a lens's distortion factors is known as lens calibration. Once the distortions of a lens are known the image can be processed with image warping software to remove the measured distortions. In aerial photogrammetry, the calibration process is generally performed quite accurately in a laboratory and the parameters of the calibration are included with the camera. Various methods to measure the distortions of a lens can be applied, such as a slide with a grid marked on it can be placed in the film aperture, a light shone through it and the projected image measured. With satellite sensors the calibration process can be performed in laboratory before the flight, such as in aerial photogrammetry or after the flight with real data set (Breton *et al.*, 2002). The first solution can only be performed by the owner of the satellite before the launch. The second solution can be performed after the satellite launch either by the owner of the satellite during the first months of the mission (Begni *et al.*, 1984) or afterwards by the users in an auto- (or self-) calibration process (Kornus *et al.*, 2006)

The lens calibration addressed different systematic errors, such as the principal point displacement, the focal length variation, the radial symmetric distortions, the decentering lens distortion (or the radial-asymmetric and tangential distortions), the scale variation in CCD line direction and the CCD line rotation in the focal plane. Some of these distortions do not apply for linear array push-room scanners, such as the tangential distortions or some have a negligible impact on the image geometry, such as the scale variation in line direction.

Most of these principal distortions (principal point displacement, focal length variation, CCD line rotation, etc.), through an auto-calibration, were already included and corrected into the 3D physical multi-sensor geometric modelling developed at the Canada Centre for Remote Sensing (CCRS) (Toutin, 1995, 2006). In fact, their effects are correlated with some other external orientation parameters and thus corrected when using an integrated geometric modelling where the full geometry of viewing (platform+sensor+Earth) is considered. The only remaining lens distortions, not addressed by CCRS 3D physical multi-sensor geometric modelling, are the radial symmetric/asymmetric and tangential distortions because they were negligible with the previous medium-resolution sensors, such as Landsat-TM/ETM, SPOT-HRV, ASTER, IRS-C/D. The mathematical function of these remaining lens distortions is well known (Brown, 1966, Kölbl, 1971) and can be computed during an auto-calibration process.

The main objectives of this research study are to address the radial symmetric and asymmetric distortions for high-resolution sensors, and thus to perform an in-flight calibration of the high-resolution SPOT-5 HRS/HRG and Formosat-2 lenses. The other objectives are to evaluate the impacts of this in-flight calibration on the sensor orientation, 3D geometric modelling and DEM generation.

2. STUDY SITE AND DATA SET

2.1 Study Site

The study site is an area north of Québec City, Québec, Canada (47º N, 71º 30' W). This study is an urban, rural and forested environment and has a hilly topography in the south with a mean slope of 7º (Figure 1), and mountainous topography in the north with a mean slope of 10º and maximum slopes of 30º. The elevation ranges from 0 m at the St-Lawrence River to 1000-m in the Canadian Shield. Québec City is in the south-east part (Figure 2).

Figure 1. Northern winter view over snow-covered frozen lake in Beauport study site, Quebec with boreal forest and a hilly topography

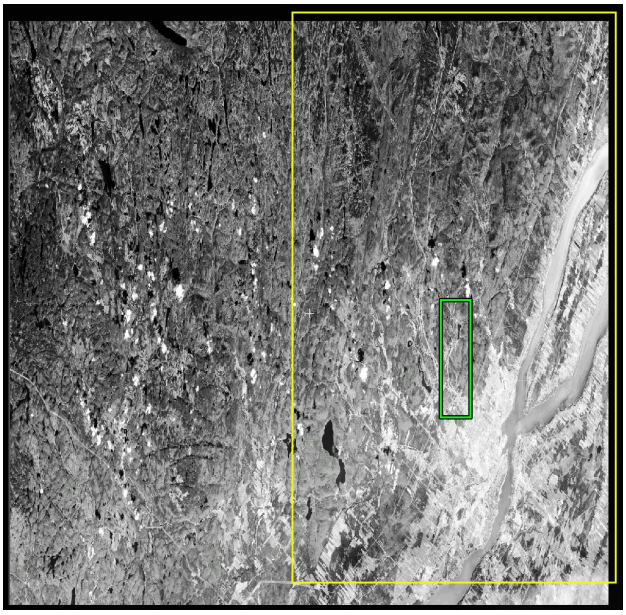

Figure 2. SPOT-5 HRS forward image, acquired north of Québec City, Canada (120 km by 60 km; 10 m by 5 m pixel spacing). The yellow box represents the across-track HRG stereo-pair (60 km by 60 km) and the green box the Lidar data (5 km by 13 km). SPOT-5 © 2003 CNES and Courtesy SPOT-Image, France

2.2 Data Set

The ±22° in-track stereo-images (120 km by 60 km; 10 m by 5 m pixel spacing; base-to-height ratio, *B/H*, of 0.85) were acquired September 18, 2003, and is a courtesy of SPOT-Image, France. The SPOT5 HRS images are raw level-1A data, orbit oriented, with detector equalization only. Ephemeris and attitude data are available in the metadata as well as general information related to the sensors and satellite. The images display 5% of clouds and their shadows (Figure 2). A second stereo-pair was later acquired over the same study site for an independent validation of the auto-calibration process.

In addition, SPOT5 HRG across-track stereo-pair (Figure 1 yellow box; 60 km by 60 km; 5 m by 5 m pixel spacing; *B/H* of 0.77) was acquired on May 5 and 25, 2003, and is a courtesy of SPOT-Image, France with viewing angles of +23º and -19º, respectively. The SPOT5 HRG images are raw level-1A data, orbit oriented, with detector equalization only. Ephemeris and attitude data are available in the metadata as well as general information related to the sensors and satellite. The May 5 image displays snow in the forests (upper part) and frozen lakes (lower left and centre), for almost 50% of the image, but not the May 25 image. These differences in snow/ice generated large radiometric differences in SPOT5 HRG stereo-images and consequently numerous mismatched areas during the image correlation process. However, the objectives of this study are not to address DEM generation process and accuracy but the impacts of the lens auto-calibration process.

Finally, an in-track panchromatic stereo-pair (Figure 3; 24 km by 24 km; 2-m pixel spacing; *B/H* of 1) was acquired December 28, 2004 by the new Taiwanese Formosat2 Remote Sensing Instrument (RSI) launched on May 21, 2004 on a sun-synchronous quasi-polar orbit at 890-km altitude (NSPO, 2006). RSI is an optical camera, which simultaneously provides high-resolution 2-m panchromatic and 8-m multiband imagery. The stereo-pair was a courtesy of the Taiwanese National Space Program Office (NSPO) and SPOT-Image, France (as distributor).

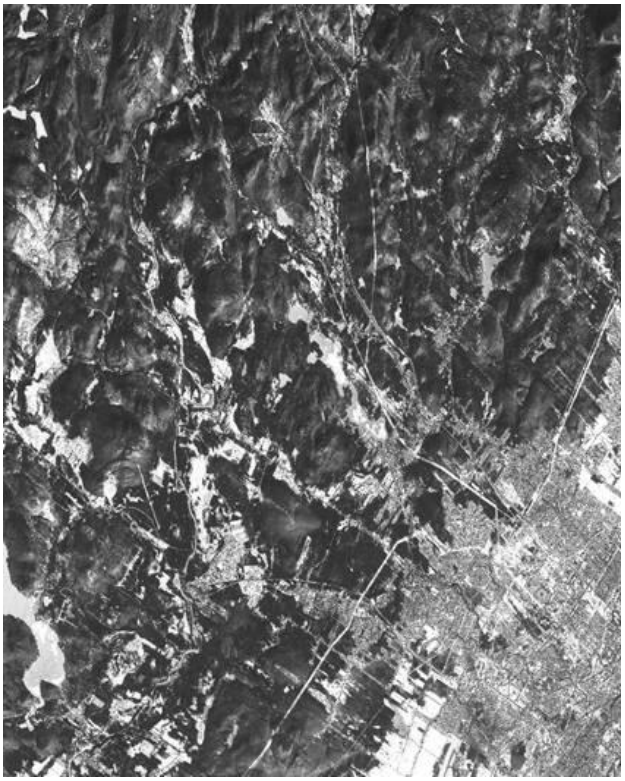

Figure 3. Forward panchromatic Formosat2 image (24 km by 24 km; 2-m pixel spacing), north of Québec City, Quebec, Canada acquired December 28, 2004. Formosat2 © National Space Program Office, Taiwan 2004, and Courtesy of SPOT-Image, France

The stereo-images are acquired along the track by pitching the RSI sensor. The Formosat-2 images are raw level-1A data, orbit oriented, with detector equalization only. Ephemeris and attitude data are available in the metadata as well as general information related to the sensors and satellite. Snow over bare surfaces as well as frozen lakes are present on the full images. However, it does not have an impact during the image matching because the wind-blown snow on large bare surfaces generating uneven surfaces as well as snowmobile and skater tracks create texture and contrast on 2-m pixel images. A third image was later acquired over the same study site for an independent validation of the auto-calibration process.

To evaluate the elevation accuracy of the stereo-extracted DEMs, accurate spot elevation data was obtained from a Lidar survey conducted by GPR Consultants (www.lasermap.com) on September 6th, 2001 (Figure 2 green box). The Optech ALTM-1020 system is comprised of a high frequency optical laser coupled with a Global Positioning System and an Inertial Navigation System (Fowler, 2001). The ground point density is about 300,000 3-D points per minute and the accuracy is 0.30 m in planimetry and 0.15 m in elevation. Since it was impossible to cover the full SPOT5 HRS stereo-pair (60 km by 120 km), ten swaths covering an area of 5 km by 13 km (Figure 2, green rectangle) and representative of the full study site were acquired. The results of the Lidar survey are then an irregular-spacing grid (around 3 m), due also to no echo return in some conditions such as buildings with black roofs, roads and lakes. Since the objectives of this research study were to evaluate the stereo DEMs, the Lidar elevation data was not interpolated into a regular spacing grid so as to avoid the

propagation of interpolation error into the checked elevation and the final evaluation of the stereo-extracted elevations.

3. EXPERIMENT

3.1 The Processing Steps

Since the processing steps of DEM generation using either in-track or across-track stereo images are well known (Toutin, 2001), the processing steps, including the accuracy evaluation can be summarized into three major steps (Figure 4):

1st Step: Acquisition and pre-processing of the remote sensing data (images and metadata) and collection of ground control points (GCPs) with their 3D cartographic coordinates and two-dimensional (2D) image coordinates. 1:20,000 digitized topographic maps (2-3 m accuracy) were used. The image pointing accuracy is half pixel but sometimes one pixel in the mountainous areas due to the GCP definition;

2nd Step: Computation of the sensor orientations (internal and external) using the CCRS satellite model, initialized with approximate parameter values computed from the meta data, and refined by an iterative least-squares stereo-bundle adjustment with the GCPs and orbital constraints. Theoretically 3-4 accurate GCPs are enough to compute the stereo model, but more GCPs were used to have an overestimation in the adjustment and to cancel the impact of random errors in the computation of the radial/tangential symmetric and tangential distortions of the lenses.

3rd Step: Extraction of elevations using an area-based image correlation process, computation and comparison of DTM with Lidar data for different land cover classes.

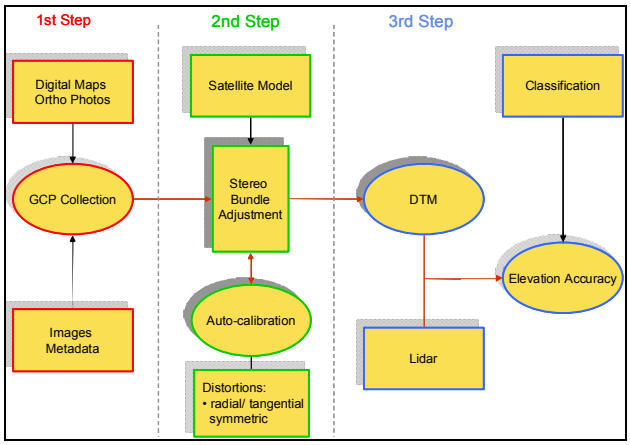

Figure 4. Processing steps for the generation of DTMs from stereo-images and their evaluation with Lidar data.

The DEM is then evaluated with the Lidar elevation data. About 5 000 000 points corresponding to the overlap area were used in the statistical computation of the elevation accuracy: the linear error with 68% confidence level (LE68). Different parameters (land cover and its surface height), which have an impact on the elevation accuracy, were also evaluated.

3.2 The Satellite Model

The satellite model is a 3D physical model originally developed to suit the geometry of pushbroom scanners, such as SPOT-HRV, and subsequently adapted as an integrated and unified geometric modelling to geometrically process multisensor images (Toutin, 1995) and HR images (Toutin, 2006). This 3D physical model applied to different image types is robust and not sensitive to GCP distribution when there is no extrapolation in planimetry and elevation. Since this modelling is well explained in the previous references, only a summary is given. The geometric modeling represents the well-known collinearity condition (and coplanarity condition for stereo model), and integrates the different distortions relative to the global geometry of viewing. This 3D physical model has been applied to medium-resolution visible and infra-red (VIR) data (MODIS, Meris, Landsat5/7, SPOT1-5, IRS1-C/D, ASTER, Kompsat-1 EOC, CBERS, ResourceSat-1), HR-VIR data (Ikonos, EROS, QuickBird, OrbView, SPOT5, Formosat-2, Cartosat), as well as radar data (ERS-1/2, JERS, SIR-C, Radarsat-1 and ENVISAT). In 2005, a preliminary adaptation of this universal geometric modelling has been realized for Formosat2. Since the attitude data were not properly recorded in the old SPOT-Image data format, the high-frequencies of the attitude variations were not taken into account in the 3D modelling: only the constant and linear parts were included. This problem should have been now resolved by SPOT-Image with the DIMAP format.

3.3 The Auto-Calibration Process

As mentioned before the CCRS geometric modelling already performed the auto-calibration of most of the systematic lens distortions: the principal point displacement, the focal length variation, the scale variation in CCD line direction and the CCD line rotation in the focal plane. Only the radial symmetric distortions and the decentering lens distortion (radial-asymmetric and tangential) were not corrected. The mathematical functions of these remaining lens distortions are, however, well known: 2D polynomial functions, with parameters and order varying as a function of the type of distortions and the lens diameter (Brown, 1966, Kölbl, 1971). They can be separately or simultaneously computed from the GCP residuals of the least square adjustment of the sensor orientations when a large number of GCPs regularly distributed in column direction are used. In fact, the GCP residuals combined a random error related to the input data and a systematic error related to these remaining lens distortions. It enabled to separate the systematic errors from the random errors by least-squares fitting the chosen mathematic function of the distortion to GCP residuals of the least-squares stereo bundle adjustment. Figure 5 is an example of the separation of the random and systematic errors by least-square fitting odd 2D 3rd-order polynomial functions to GCP residuals for computing the radial symmetric distortion of Formosat2 RSI lens.

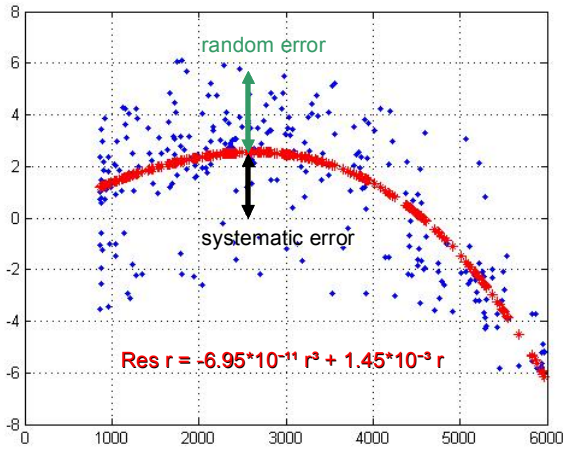

Figure 5. Computation of the radial symmetric distortion for Formosat2 RSI lens by separating random and systematic errors of GCP residuals: the radius r (in pixel) for *x*-axis and residual/error (in pixel) for *y*-axis.

Depending on the sensor, the lens, the position of CCD in the focal plane, the number of CCDs and the size of the lens, some of these remaining lens distortions, if not all, could have a negligible impact in comparison to the sensor resolution and the final expected accuracy of sensor orientations. In general, the radial symmetric distortions have a predominant effect over the decentering lens distortions. In addition, the tangential distortion as part of the decentering lens distortions is also negligible for a push-broom scanner due to its uni-dimensional geometry.

After performing different tests to compute the mathematical functions of these distortions for the three evaluated HR sensors, SPOT5 HRS, SPOT5 HRG and Formosat RSI, it was found that:

1. The tangential distortion of the decentering lens distortions for SPOT5 HRS is negligible and the radial asymmetric is very small (1/5 of a pixel) but can be considered;
2. All distortions for SPOT5 HRG 5-m are negligible;
3. The two parts of the decentering lens distortions for Formosat RSI are negligible.

Consequently, SPOT5 HRS will be corrected for radial symmetric and asymmetric distortions (Figure 6), Formosat RSI for radial symmetric distortion (Figure 5) but SPOT5 HRG is not corrected for any distortion. Since Formosat-2 uses the same lens to acquire the stereo-images, the data of both images can be combined for the computation of the mathematical functions representing the radial symmetric distortion. On the other hand, two distinct cameras and lenses are used for acquiring the two images of the stereo-pair: each lens does have a different, but quite similar, 1D 3rd-order polynomial function curve and should be computed separately.

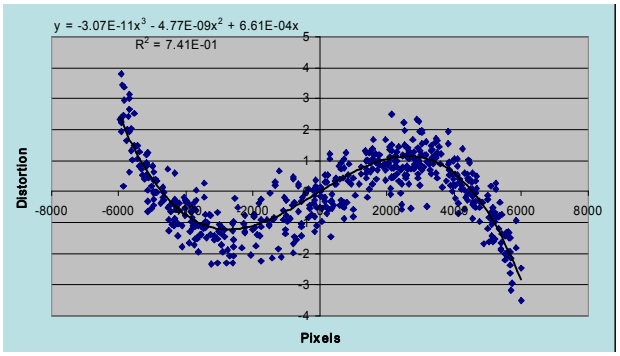

Figure 6. Computation of the combined radial symmetric and asymmetric distortions for the forward SPOT5 HRS lens by separating random and systematic errors of GCP residuals: the radius r (in pixel) for *x*-axis and residual/error (in pixel) for *y*-axis.

When correcting for the HRS lens distortions with the auto-calibration, the errors become thus random (Figure 7) with a root mean square distortion of 0.5 pixel, corresponding to the input error. Same results applied for Formosat-2 RSI data. It then justifies *a posteriori* the effectiveness of the corrections. In addition, these lens distortion corrections were applied to other independent images (SPOT5 HRS and Formosat-2 RSI) acquired over the same study site and an other study site, showing large improvements in the accuracy of sensor orientations.

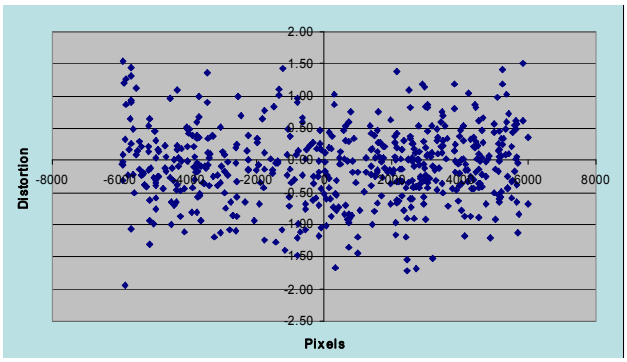

Figure 7. Remaining errors after correcting the radial symmetric and asymmetric distortions of the forward SPOT5 HRS lens showing only random error: the radius r (in pixel) for *x*-axis and error (in pixel) for *y*-axis.

4. IMPACTS OF THE AUTO-CALIBRATION

4.1 On Sensor Orientations

Tables 1 and 2 summarize the impacts of the auto-calibration process on sensor orientations for the different SPOT5 HRS and Formosat-2 RSI images, respectively. The results are GCP RMS residuals given in the image space (*x* column and *y* row in pixel).

Auto-calibration		Without	With	Improvement
1st Forward	*x*	1.1	0.5	55%
	y	1.3	1.1	15%
1st Backward	*x*	1.1	0.6	45%
	y	1.2	1.1	8%

2nd Forward	*x*	1.1	0.4	64%
	y	0.9	0.8	11%
2nd Backward	*x*	1.0	0.4	60%
	y	0.9	0.7	22%

Table 1. Impact of the auto-calibration on sensor orientations of the SPOT5 HRS forward/backward images of the two stereo-pairs with the RMS residuals at GCPs in the image space (*x*-column and *y*-row in pixel) and the improvement (in percentage)

Table 1 shows larger improvements (over 55%) in the *x*-direction than (10-20%) in the *y*-direction: this is mainly due by the fact that the CCDs are aligned in the *x*-axis of the focal plane, resulting in radial symmetric and asymmetric distortions mainly in the column direction. It should be noted that half pixel in the column direction (5 m) correspond to one pixel in the line direction (5 m) due to the oversampling of the line versus the HRS sensor resolution (10 m) by a factor of two. The impact in the row direction is due to a combined effect with the CCD line rotation in the focal plane. In fact, these results correspond to half resolution of the HRS sensor in both directions. Finally, these results for SPOT5 HRS auto-calibration demonstrated (i) the range of the radial distortions to be around half and 1/10 resolution (5 m and 1 m, respectively) of the HRS sensor in *x*-column and *y*-row directions respectively, and (ii) the necessity to apply lens calibration to achieve sub-resolution accuracy for the sensor orientations. If such accuracy (5 m or better) is not requested for specific applications the lens calibration is not mandatory. In addition because the input data error (2-3 m) is included in the RMS residuals the internal accuracy of the sensor orientation is better than 5 m, in the order of one-third of resolution (Toutin, 2006).

Auto-calibration		Without	With	Improvement
1st Forward	*x*	3.1	1.5	51%
	y	1.9	1.3	32%
1st Backward	*x*	3.3	1.9	42%
	y	1.9	1.4	26%
3rd Image	*x*	2.9	1.5	48%
	y	2.0	1.5	25%

Table 2. Impact of the auto-calibration on sensor orientations of the three Formosat2 RSI images with the RMS residuals at GCPs in the image space (*x*-column and *y*-row in pixel) and the improvement (in percentage)

Table 2 shows almost the same improvements for Formosat2 RSI (around 50%) in the *x*-direction but better improvements (more than 25%) in the *y*-direction than for SPOT5 HRS results (Table 1). This is mainly due by the fact that the panchromatic CCDs are ex-centred in the focal plane resulting in radial symmetric distortion in both directions, which explained the larger improvement in *y*-direction. In addition, the impact in the row direction is also combined with the CCD line rotation in the focal plane. These medium-quality results are mainly due to: (i) the inconsistent attitude data, whose high frequencies were not applied in the sensor orientation, and (ii) the 2-3 m error of the input data, which were not precise enough when compared to RSI sensor resolution (2 m). Even if sub-pixel accuracy could have been achieved by integrating the high frequencies of attitude data, such as the results obtained using CCRS multi-sensor geometric model with other sensors (Toutin, 1995, 2006), these 1.5-pixel accurate results are similar and even better than those obtained (2 pixels) on an other study using also a rigorous sensor model (Chen *et al.*, 2006). These results for Formosat2 RSI auto-calibration demonstrated (i) the range of the radial distortions to be around 1-2 and 0.5 resolutions of the RSI sensor in *x*-column and *y*-row directions respectively, and (ii) the necessity to apply lens calibration to achieve sub-resolution accuracy for the sensor orientations. If such accuracy (3 m or better) is, however, not requested for specific applications the lens calibration is not mandatory. In addition because the input data error (2-3 m) is included in the RMS residuals the internal accuracy of the sensor orientation is better than 1.5 resolutions (3 m), in the pixel/sub-pixel range (Toutin, 1995).

4.2 On DEM Generation

The second results are the quantitative evaluations of two DSMs extracted from the first HRS and RSI stereo pairs. The evaluations are related to the matching successes, the RMS error when compared to GCP elevation and to the comparison of DSMs with Lidar elevation data to compute LE68 (Table 3). About 5 000 000 points were used for the LE68 computation over the entire overlap areas. Because the stereo-pairs and the Lidar data were acquired at different seasons with different planimetric resolutions, the compared elevations do not always exactly correspond to the same ground point and elevation; in fact the height, or a part, of the different surfaces (trees, buildings, etc.) is differently included in the elevation (Figure 8). LE68 was thus computed for the bare soils where there is no height differences between the two compared ground-point elevations.

Stereo Pair	SPOT5 HRS		Formosat2 RSI	
Calibration	Without	With	Without	With
Mismatched area	20%	20%	7%	4%
RMS Error versus GCPs	4.8 m	4.1 m	4.3 m	3.5 m
LE68 Total	6.1 m	5.9 m	12.0 m	7.2 m
LE68 Bare Soils	3.5 m	3.2 m	9.7 m	3.8 m

Table 3. Error results on elevation extracted from SPOT5 HRS/Formosat2 RSI stereo-images without and with auto-calibration: Percentage of mismatched areas, RMS errors (in metre) when compared to GCP elevation, LE68 (in metres) for the entire overlap areas and the bare soils when compared to Lidar elevation data

Table 3 showed that the comparison of results (without versus with) are quite different for HRS and RSI. This is mainly due to the location of CCDs in their respective focal planes: centred and aligned in *x*-direction for HRS versus off-centred in *y*-direction for RSI. In addition, the better results with HRS (sub-pixel) than with RSI (1-2 pixels) with a similar *B/H* ratio are still due to the inconsistent attitude data and the non-integration in the sensor orientations of their high-frequencies. Better results (in the order of sub-pixel) should be expected in the future.

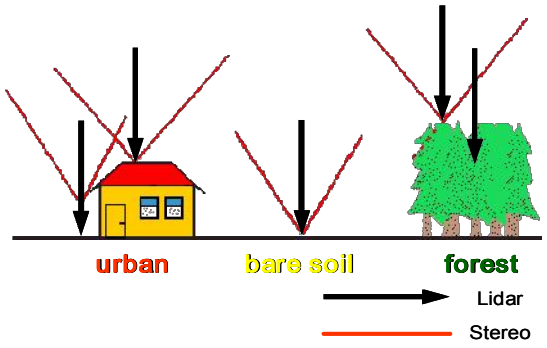

Figure 8. Comparison of stereo-extracted and Lidar elevations

While the 20% mismatched areas for SPOT5 correspond to clouds and shadows, the matching has then a very high success rate (98%) in the other areas. It is mainly due that there is no transversal parallax between the quasi-epipolar images, resulting from a (sub-)pixel accurate stereo-modelling (Table 1). In addition, the radial distortion is mainly in *x*-column (Table 1) while the elevation parallaxes are in *y*-row for in-track stereoscopy: it does explain the small impact of radial distortions on elevation extraction and thus the small improvements (0.2-0.7 m) of the three elevation errors between without and with auto-calibration.

When processing Formosat2 without auto-calibration, some transversal parallaxes (4-6 lines) between the quasi-epipolar images have been introduced by the 2-resolution accuracy of the stereo-modelling and by the larger radial distortions proportionally to the resolution. These parallaxes explain then the larger seven per cent of mismatched areas. On the other hand, the larger errors in the three elevation errors without auto-calibration result that the *y*-row component of radial distortions is in the same direction than the elevation parallaxes with in-track stereoscopy.

It should also note that the improvements using auto-calibration for both sensors are not as good for elevation in the correlation process (Table 3) than for planimetric positioning in the sensor orientation (Table 1). The main reason is that the radial distortions degraded more the planimetry of the sensor orientations while being in the same direction only small differential elevation parallaxes for an image conjugate point remain and affected the elevation extraction. The major consequence is that auto-calibration for DEM generation is thus more important to perform in high relief areas where planimetric errors have an important impact on elevation errors.

5. CONCLUSIONS

The main objectives of this research study were to address the internal orientations of high-resolution sensors, and to perform an in-flight calibration of the high-resolution SPOT5 HRS/HRG and Formosat2 RSI lenses. The other objectives were to evaluate the impacts of this in-flight calibration on the sensor orientations, 3D geometric modelling and DEM generation. Stereo-extracted elevations were compared to accurate Lidar elevation data. Since the CCRS 3D multi-sensor geometric modelling used in the auto-calibration already corrects some of the lens distortions (Toutin, 1995), only the remaining radial and decentering distortions were addressed in this study.

The first results on the lens distortion computation and evaluation have shown that:

1. The tangential distortion of the decentering lens distortions for SPOT5 HRS was negligible and the radial asymmetric is very small (1/5 of a pixel) but can be considered;
2. All distortions for SPOT5 HRG 5-m were negligible; and
3. The two parts of the decentering lens distortions for Formosat RSI were negligible.

The results on the sensor orientations with the 3D geometric model computation also demonstrated that the auto-calibration improve the sensor orientation around 50-60% and 10-30% in *x*-column and *y*-row, respectively depending of the sensor and its location in the focal plane. These results demonstrated thus the necessity of the auto-calibration process for SPOT5 HRS and Formosat2 RSI to obtain sub-pixel accuracy in the planimetric positioning.

The last results on the stereo-extraction of elevations compared to Lidar elevation data for the total overlap areas and the bare soils demonstrated few improvements (less than 0.5 m) for SPOT5 HRS because the radial distortions were in the *x*-column while the elevation parallaxes were in the y-row direction with in-track stereo-images. This same reason also applied to Formosat2 RSI but the *y*-row component of radial distortions due to its off-centred location in the focal plane generated larger elevation errors (5 m and more), which were then corrected by the auto-calibration process.

Finally, if sub-pixel accuracy (planimetry and elevation) is not requested for specific applications, the lens calibration could be neglected without degrading the final results more than one pixel. However, the auto-calibration process should be always performed for DEM generation in mountainous areas because the radial distortions affected the sensor orientation (few pixels), which will have a large impact on elevation. Worse relative results were obtained with Formosat2 than with SPOT5 because there were some inconsistencies in attitude data of our Formosat2 data set. These problems should have been now resolved with the new DIMAP format of SPOT-Image.

ACKNOWLEDGEMENTS

The authors thank Mr. Marc Bernard and Mr. Didier Giacobbo of SPOT-IMAGE, France for the SPOT5 HRS/HRG and Formosat2 RSI stereo pairs, Mr. Réjean Matte du *Ministère des Ressources naturelles du Québec*, Canada for the topographic data, the company GPR Consultants, Canada for the Lidar survey. They also thank the Canadian Space Agency, and especially M. Paul Briand, for their financial support in the SPOT5 experiment under the Government Related Initiative Program.

REFERENCES

Breton, E., A. Bouillon, R. Gachet, F. Delussy, 2002, Pre-flight and in-flight geometric calibration of SPOT5 HRG and HRS images, *Pecora 15/Land Satellite Information IV/ISPRS Commission I/FIEOS 2002 Conference Proceedings,* CD-ROM.

Brown, D.C., 1966, Decentering distortion of lenses, *Photogrammetric Engineering*, 32(3), pp. 444-462.

Begni, G, D. Léger, M. Dinguirard, 1984, An In-Flight Refocusing Method for the SPOT-HRV Cameras, *Photogrammetric Engineering & Remote Sensing*, 50(12), pp. 1697-1705.

Chen, L.-C., T.-A. Teo, C.-L. Liu, 2006. The Geometrical Comparisons of RSM and RFM for FORMOSAT-2 Satellite Images, *Photogrammetric Engineering & Remote Sensing*, 72(5), pp. 573-579.

Fowler, R.A., 2001. The Thorny Problem of Lidar Specifications, *Earth Observation Magazine*, 10(4), pp. 13-17.

Kölbl, O., 1971, Verzeichnungsdarstellung bei der vollständigen Kalibrierung, *Bildmessung und Luftbildwesen*. vol. 39, pp. 169-176.

Kornus, P., R. Alamús, A. Ruiz, J. Talaya, 2006, DEM generation from SPOT 5 three-fold along-track stereoscopic imagery using autocalibration, *ISPRS Journal of Photogrammetry and Remote Sensing,* 60(3), 147-159.

NSPO, 2006. Formosat-2 Remote Sensing Mission, URL: http://www.nspo.org.tw/2005e/projects/project2/intro.htm (accessed 12 May 2006).

Toutin, Th., 2006. Generation of DSM from SPOT-5 in-track HRS and across-track HRG stereo data using spatiotriangulation and autocalibration, *ISPRS Journal of Photogrammetry and Remote Sensing*, 60(3), 170-181.

Toutin, Th., 2001. Elevation modelling from satellite visible and infrared (VIR) data: a review, *International Journal of Remote Sensing*, 22(6), pp. 1097-1125.

Toutin, Th., 1995. Generating DEM from Stereo-Images with a Photogrammetric Approach: Examples with VIR and SAR data, *EARSeL Advances in Remote Sensing*, 4(2), pp. 110-117.